Journal of the European Ceramic Society **11** (1993) 35–41

A Theoretical Evaluation of the Stability of Sialon-bonded Silicon Carbide in the Blast Furnace Environment

D. A. Gunn

Hepworth Refractories Ltd, Central Research Laboratories, Worksop, Nottinghamshire S80 3EU, UK

(Received 13 January 1992; revised version received 27 February 1992; accepted 22 April 1992)

Abstract

A theoretical study is described on the effect of alkali attack on the sialon bond ($Si_{6-z}Al_zO_zN_{8-z}$) in silicon carbide refractories in the blast furnace environment. Phase diagram and thermochemical relationships indicate that raising the z-number of the sialon will confer increased resistance to alkali attack, due to the formation of higher melting point reaction products in the alkali condensation zone. However, at z-numbers greater than two there is also a greater possibility of deleterious α- and β-alumina formation in the lining. Theoretical and practical considerations indicate that the optimum bond composition to use in the lower stack is a sialon with a z-number of two.

Es werden theoretische Untersuchungen über den Einfluß des alkalischen Angriffes auf den Sialon-Binder ($Si_{6-z}Al_zO_zN_{8-z}$) in Siliziumcarbid-Feuerfestmaterial für die Umgebung des Hochofens beschrieben. Das Phasendiagramm und thermochemische Beziehungen weisen darauf hin, daß ein höherer z-Index in der Stöchiometrie des Sialons zu einer verbesserten Beständigkeit gegen alkalischen Angriff auf Grund der Bildung von Reaktionsprodukten mit höherem Schmelzpunkt in der Alkali-Kondensationszone führt. Bei z-Indizes oberhalb von zwei kommt es jedoch zu einer höheren Bildungswahrscheinlichkeit von schädlichem α- und β-Aluminiumoxyd in der Hochofenauskleidung. Theoretische und praktische Betrachtungen zeigen, daß die optimale Zusammensetzung des Bindermaterials für den Gebrauch im unteren Bereich bei einem z-Index von zwei liegt.

Cet article décrit une étude théorique de l'attaque alcaline des liaisons chimiques de type sialon ($Si_{6-z}Al_zO_zN_{8-z}$) dans des réfractaires en carbure de silicium soumis à l'environnement agressif des hauts fourneaux. L'analyse des diagrammes de phase et l'examen des relations thermo-chimiques indique qu'une augmentation de la valeur de z induit une meilleure résistance du réfractaire aux attaques alcalines. En effet, au niveau de la zone de condensation des alcalins, le point de fusion du produit obtenu après réaction est plus élevé. Cependant, si la valeur de z est supérieure à 2, on peut craindre la formation indésirée d'alumine α et β au niveau du revêtement. Des considérations théoriques et pratiques indiquent que la composition optimum correspond à un sialon de z = 2 pour les empilages.

1 Introduction

Potassium compounds present in the burden introduced into the blast furnace can be reduced to potassium vapour in the melting zone. Further reactions can occur with carbon monoxide (CO) as the gases ascend the stack to form molten potassium carbonate (K_2CO_3); or with SiO_2 and Al_2O_3 in the burden or refractory lining to form low melting alkali silicate and aluminosilicate compounds.

Nitride-bonded silicon carbide refractories are often used in the stack to counter the alkali attack problem but with limited success. Sialon-bonded silicon carbide refractories appear to offer more alkali resistance, especially as the *z*-number is raised. The possible reasons for this protective effect will be discussed in the following section. A dual approach has been attempted, where available data have allowed, to provide a wider interpretation of the sialon stability by (1) a phase diagram study assuming that the sialon bond becomes fully oxidised and then suffers an increasing degree of alkali attack, and (2) a thermodynamic interpretation involving Ellingham-type plots of oxygen potential versus temperature with labelled stability fields.

The present theoretical evaluation does not take

Journal of the European Ceramic Society 0955-2219/93/$6.00

into account the possibility of stress build-up in the lining due to the volume expansions involved when the various potassium aluminosilicates are formed. Similarly, no account has been taken of alkali, sialon and atmosphere interactions with the SiC-grain material in the refractory. In the phase diagram study, to simplify the representation of the figures, only the liquidus and solidus lines have been drawn.

The general composition of a sialon can be represented by the formula $Si_{6-z}Al_zO_zN_{8-z}$ and changes in z-number reflect the amount of substitution of Al and O for Si and N in the β-silicon nitride (Si_3N_4) lattice. To highlight possible compositional changes in the lining during oxidation and alkali attack, a range of sialon z-numbers from zero to four has been examined.

In the case of the Ellingham plots, the approximate prevailing atmosphere in the lower stack of the blast furnace has been assumed to consist of 1·7 atm (0·17 MPa) of nitrogen, 0·8 atm (0·08 MPa) of carbon monoxide and 0·01 atm (0·001 MPa) of potassium vapour gas. A secondary carbon monoxide partial pressure (P_{CO}) line has been plotted on the diagrams at 0·01 atm (0·001 MPa) to show the effect of lower P_{CO} pressure within the porosity of the brickwork.

A system of shorthand for the various compound formulae has been used throughout the discussion, e.g. potash feldspar or $K_2O.Al_2O_3.6SiO_2$ is written as KAS_6. Similarly, the notation in brackets after the element or compound denotes the physical form of the phase, e.g. KAS_6(s) refers to solid potash feldspar, just as (l) would refer to liquid and (g) to gaseous phases.

2 Discussion

The interpretation follows similar lines as previously explored by Smith & White[1] by starting from the K_2O–Al_2O_3–SiO_2 phase diagram.[2] The diagram has been simplified in Fig. 1 to show only the solid-phase relations and how the various z-number sialons change in composition as they oxidise and react with potassium vapour. Each sialon with its respective z-number has been examined in turn and the pros and cons of their suitability discussed as a possible refractory bond material in the blast furnace environment. The dashed lines across Fig. 1 have been drawn as a series of pseudobinary sections for each z-number sialon and the liquidus and solidus boundaries labelled.

2.1 Sialon $z=0$ (Si_3N_4)

Figure 2 shows the liquidus and solidus relations for Si_3N_4 without any Al and O substitution in the lattice, i.e. for $z=0$. It can be seen immediately that under severe oxidising and alkali attack conditions very low melting and low viscosity potassium silicate melts will be formed above 770°C. The presence of these melts in the nitride-bonded silicon carbide brickwork would be expected to adversely affect the life of the lining.

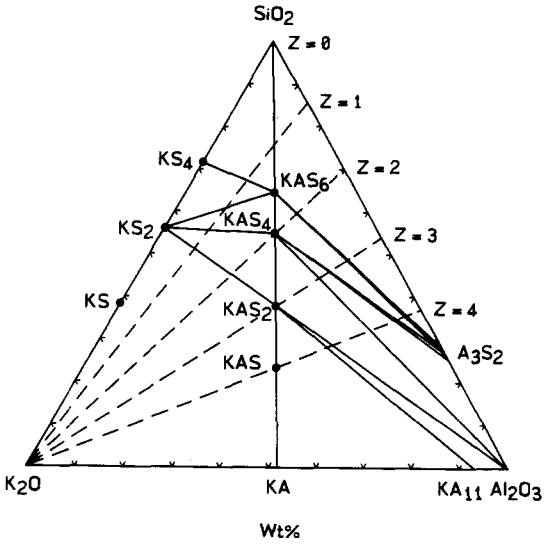

Fig. 1. Solid-phase relations in the system K_2O–Al_2O_3–SiO_2, showing changes in composition of various z-number sialons as they oxidise and pick up K_2O. K = K_2O, A = Al_2O_3, S = SiO_2.

Figure 3 for $z=0$ or Si_3N_4 shows plots of oxygen potential ($RT \ln P_{O_2}$) against temperature for the four main equilibria, for example:

$$4K(g) + 8SiO_2 + O_2 = 2KS_4(l) \qquad \text{Plot 2}$$

$$0{\cdot}45K(g) + 0{\cdot}0118Si_{76}N_{100}O_2 + O_2 = 0{\cdot}22KS_4(l) + 0{\cdot}59N_2 \qquad \text{Plot 6}$$

$$0{\cdot}57K(g) + 0{\cdot}57Si_2N_2O + O_2 = 0{\cdot}29KS_4(l) + 0{\cdot}57N_2 \qquad \text{Plot 6A}$$

$$0{\cdot}67Si_2N_2O + O_2 = 1{\cdot}33SiO_2(s) + 0{\cdot}67N_2 \qquad \text{Plot 9}$$

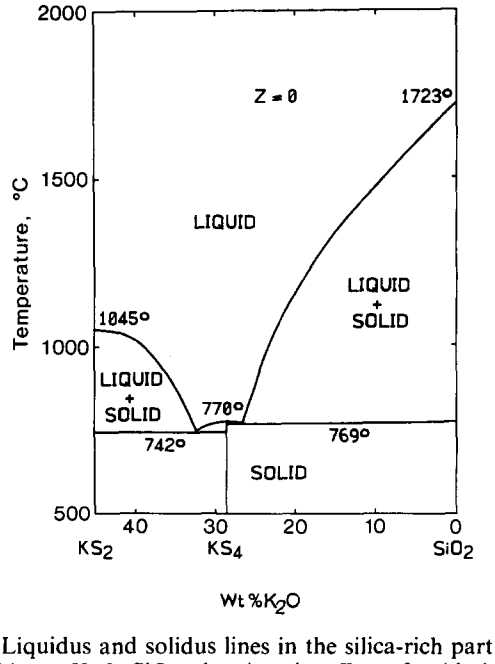

Fig. 2. Liquidus and solidus lines in the silica-rich part of the pseudobinary K_2O–SiO_2, showing the effect of oxidation and K_2O on Si_3N_4 (equivalent to a sialon with $z=0$).

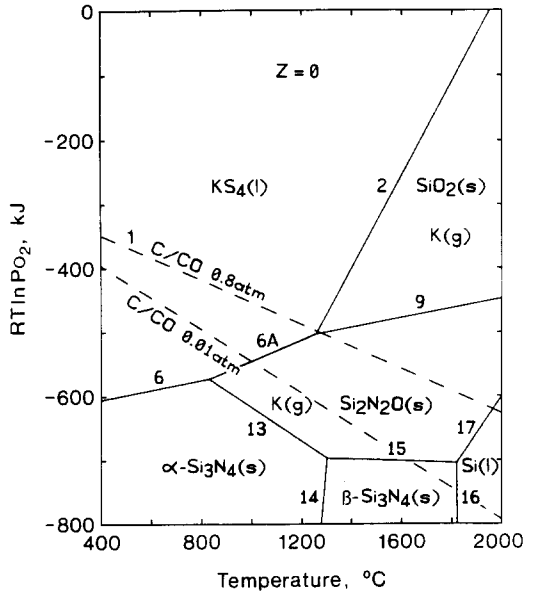

Fig. 3. Oxygen potential–temperature diagram, showing the stability fields for silicon nitrides in the presence of potassium silicates in the system K–Si–N–O at $P_{CO} = 0{\cdot}8$ and 0·01 atm, $P_{N_2} = 1{\cdot}7$ atm and $P_K = 0{\cdot}01$ atm.

Additional equations, oxygen potentials and references are listed in the thermodynamic database in the Appendix. The plots outline the limits of the stability fields for the labelled phases, e.g. liquid $KS_4(l)$ is stable in the area to the left-hand side of plots 2 and 6. The C/CO line (plot 1), representing a typical P_{CO} of 0·8 atm in the blast furnace atmosphere,[1] traverses the stability fields with rise in temperature. At a P_{CO} of 0·8 atm, and higher hot-face temperatures than about 1250°C, potassium vapour and solid silicon nitrides will be the stable phases and molten potassium silicates will not be formed. However, below 1250°C, either behind the hot face of the brick or in the cooler parts of the furnace, molten silicates will form from reactions between the potassium vapour and the Si_3N_4 bond. This effect will lead to strength weaknesses in the bricks and premature wear in the lining.

2.2 Sialon $z = 1$ (Si_5AlON_7)

For a sialon bond with $z = 1$ the reaction path results in the formation of many low-temperature silicate phases, as can be seen in Fig. 4, and consequently it was not possible to construct a corresponding stability diagram. Nevertheless, the pseudobinary indicates that alkali attack would produce phases in the brick which would be semi-molten above 700°C and completely molten above 1200°C. Even if less alkali attack is assumed above 1200°C due to the volatilisation of potassium vapour, sufficient melt formation would occur at lower temperatures to cause damage to the lining. The presence of more viscous potassium aluminosilicate compounds[3] suggests that the weakening effect should not be as great as in the equivalent nitride-bonded material described in Section 2.1.

2.3 Sialon $z = 2$ ($Si_4Al_2O_2N_6$)

As the sialon z-number is increased to 2 a noticeable change becomes apparent in the melting relationships, as shown in Fig. 5. Both the solidus and liquidus lines have risen considerably, thus making the brick much less prone to degradation by melt

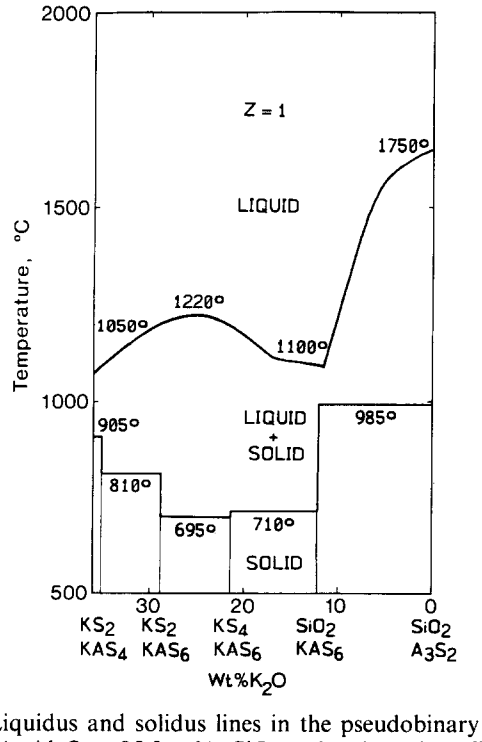

Fig. 4. Liquidus and solidus lines in the pseudobinary K_2O–(14·5 wt% Al_2O_3 + 85·5 wt% SiO_2), showing the effect of oxidation and K_2O on a sialon with $z = 1$ (Si_5AlON_7).

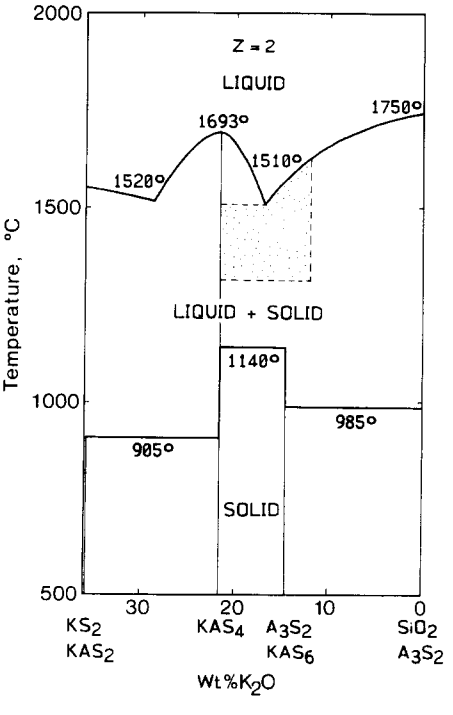

Fig. 5. Liquidus and solidus lines in the pseudobinary K_2O–(29·8 wt% Al_2O_3 + 70·2 wt% SiO_2), showing the effect of oxidation and K_2O on a sialon with $z = 2$ ($Si_4Al_2O_2N_6$). The stippled area represents the presence of alumina phase.

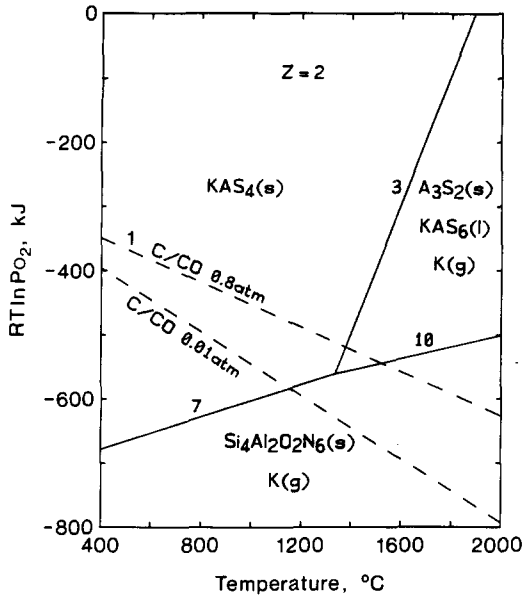

Fig. 6. Oxygen potential–temperature diagram, showing the stability field for sialon $z = 2$ ($Si_4Al_2O_2N_6$) in the presence of potassium aluminosilicates in the system K–Si–Al–O–N at $P_{CO} = 0{\cdot}8$ and 0·01 atm, $P_{N_2} = 1{\cdot}7$ atm and $P_K = 0{\cdot}01$ atm.

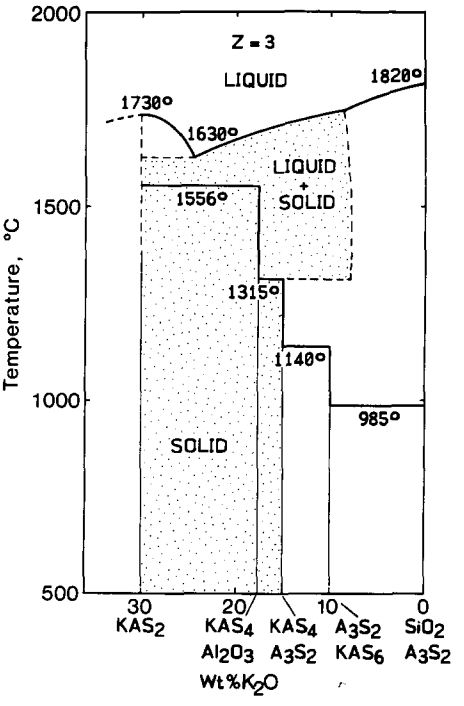

Fig. 7. Liquidus and solidus lines in the pseudobinary K_2O–(45·9 wt% Al_2O_3 + 54·1 wt% SiO_2), showing the effect of oxidation and K_2O on a sialon with $z = 3$ ($Si_3Al_3O_3N_5$). The stippled area represents the presence of alumina phase.

formation due to alkali attack in an oxidising atmosphere. If KAS_4 is assumed to be the stable phase (KAS_4 has been reported from slagged blast furnace refractories[4]) then complete melting would occur as high as 1693°C. According to the phase diagram, it is possible that Al_2O_3 could be formed at higher temperatures but would redissolve in the melt on cooling.

The stability diagram in Fig. 6 gives a more complete picture by indicating that the stable phase below about 1380°C (at a P_{CO} of 0·8 atm) is solid KAS_4. Even above this temperature, between about 1380 and 1550°C on the diagram, the sialon reaction products are comparatively high melting and therefore less prone to deformation. Above 1550°C the C/CO atmosphere line at $P_{CO} = 0{\cdot}8$ atm crosses into the sialon $z = 2$ stability field. It is interesting to note that at lower P_{CO} levels, for example at $P_{CO} =$ 0·01 atm within the brickwork, the C/CO line traverses the solid KAS_4 and sialon fields without entering the silicate field (on the upper right-hand side of Fig. 6), which could contain some minor amounts of liquid phase. The presence of predominantly *solid* reaction products over the entire temperature range would explain the observed resistant behaviour of $z = 2$ sialon-bonded silicon carbide refractories to alkali attack.

2.4 Sialon $z = 3$ ($Si_3Al_3O_3N_5$)

At a sialon z-number of 3 in Fig. 7, KAS_2 can be taken to be the major phase with a high melting point of above 1700°C. Both solidus and liquidus curves have risen to nearly meet each other, thus resulting in a bond material that should be resistant to melt formation when subjected to alkali attack over the complete temperature range. Unfortunately, free α-alumina will be liberated in the brick during alkali attack. The presence of this material in the blast furnace lining in alkali condensation areas has always been viewed with suspicion due to its melt-forming properties. Another factor that should be considered is that raising the z-number of sialon-bonded silicon carbide bricks to higher values causes the product to sinter increasingly well during firing which can produce materials more susceptible to thermal shock damage.

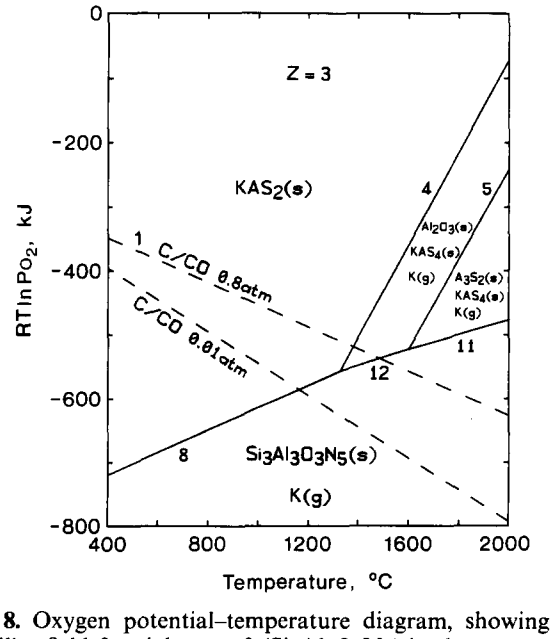

Fig. 8. Oxygen potential–temperature diagram, showing the stability field for sialon $z = 3$ ($Si_3Al_3O_3N_5$) in the presence of potassium aluminosilicates in the system K–Si–Al–O–N at $P_{CO} = 0{\cdot}8$ and 0·01 atm, $P_{N_2} = 1{\cdot}7$ atm and $P_K = 0{\cdot}01$ atm.

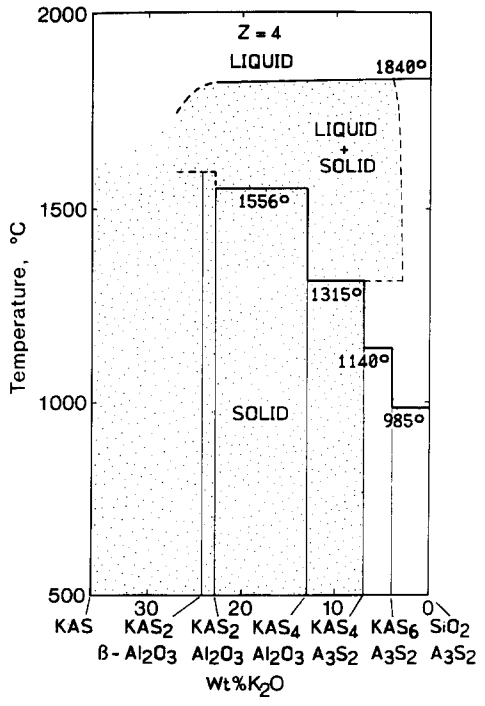

Fig. 9. Liquidus and solidus lines in the pseudobinary K_2O–(62·9 wt% Al_2O_3 + 37·1 wt% SiO_2), showing the effect of oxidation and K_2O on a sialon with $z = 4$ ($Si_2Al_4O_4N_4$). The stippled area represents the presence of alumina phases.

The stability diagram for sialon $z = 3$ in Fig. 8 is very similar to the previous $z = 2$ diagram in that high melting solid phases will be formed when the sialon is subjected to oxidation and alkali attack. The only major difference is the possibility of free α-alumina formation in the lining at the typical P_{CO} pressures found in the blast furnace. At lower P_{CO} pressures deeper within the brick, α-alumina is less likely to occur.

2.5 Sialon $z = 4$ ($Si_2Al_4O_4N_4$)

Finally, at a sialon z-number of 4 in the pseudobinary drawn in Fig. 9, KAS is the major phase and all the alkali attack reaction products are high melting. Again there is the problem of α-alumina formation and the additional problem of 'β'-alumina ($K_2O.11Al_2O_3$, the potassium equivalent of β-alumina) formation which involves a volume increase that is often accompanied by crack formation.[4] It should be remembered that in this high potash region the K_2O–Al_2O_3–SiO_2 ternary system is incomplete and the pseudobinary drawn in Fig. 9 above about 22% K_2O is only approximate, as indicated by the dashed lines.

An equivalent stability diagram for sialon $z = 4$ has not been drawn because of the lack of available thermodynamic information in the literature.

3 Practical Considerations

A series of experimental bricks were pressed and fired in nitrogen with z-numbers of 0, 1·0, 1·5, 2·0 and 2·5. Their physical properties showed no particular trends apart from the end members, e.g. $z = 0$ and $z = 2·5$, as shown in Table 1.

Table 1. Fired physical properties

z-Number	*Bulk density* (kg/m^3)	*Open porosity* (%)	*Ambient MOR* (*MPa*)
0	2690	14·9	44
1·0	2750	13·1	36
1·5	2750	13·3	46
2·0	2720	13·0	38
2·5	2800	10·8	48

An important feature common to all these bricks was the uniformity of the sialon composition or z-number throughout the brick sections. Several similarly manufactured products from other sources show a fall in z-number towards their internal core regions, e.g. from $z = 2$ to $z = 0·5$ in one case.

However, more significantly for this work, the bricks were also subjected to a molten alkali resistance test which evaluates the properties of refractory brick both before and after exposure to molten potassium carbonate (in the presence of carbon granules) at 925°C. The results of the test have been listed in Table 2.

The fall in strength of samples with $z = 0$ after the alkali resistance test could be associated with their higher open porosities which would allow easier access and corrosion by molten alkali. The high level of strength improvement for $z = 1$ samples may be associated with the formation of low melting glasses at 925°C (as discussed in Section 2.2) which would be frozen during the modulus of rupture (MOR) test at ambient temperatures. Hot strength measurements are not usually carried out at higher temperatures under these conditions due to the possibility of alkali attack damage to the test equipment. An overall improvement in three-point bend strength with rise in z-number was observed after the test. The lower z-number bricks tended to lose weight which could cause a loss in bond strength under service conditions, while the higher z-numbers increased in weight, probably due to the absorption of alkali and the formation of compounds.

From these results and the physical properties it was decided to select $z = 2$ as the optimum

Table 2. Molten alkali resistance test at 925°C

z-Number	*% MOR change*	*% Weight change*
0	−10·7	−2·51
1·0	+24·0	−1·43
1·5	+0·1	−0·84
2·0	+0·8	+0·58
2·5	+3·9	+1·05

composition to resist molten alkali attack in the blast furnace environment.

4 Conclusions

(1) From a theoretical and melting relationship standpoint, in a typical blast furnace environment, a silicon carbide lining containing a sialon bond with $z=2$ appears to offer the most resistance to alkali attack. This is brought about by the formation of high melting point reaction products within the bond which would be solid in the normal molten alkali condensation zone. In addition, the precipitation of free alumina in the brick structure is unlikely to occur at this z-number.

(2) The increase in alkali resistance with rise in sialon z-number can be explained by the gradual shift in the composition of the oxidised reaction products towards higher melting point potassium aluminosilicate compounds.

(3) During service alkali attack on sialon compositions with z-numbers greater than two will cause the melting point of the reaction products to rise to a maximum but at the same time deleterious α- and possibly β-aluminas will appear in the brick microstructure.

(4) Practical considerations, primarily from the results of a molten alkali resistance test, also confirm that the optimum matrix bond composition to use in the blast furnace lower stack is a sialon with a z-number of two.

References

1. Smith, P. L. & White, J., Stability relationships of silicon carbide and silicon nitrides and their bearing on performance in blast furnace environments. *Trans. J. Brit. Ceram. Soc.*, **82** (1983) 23–30.
2. Levin, E. M., Robbins, C. R. & McMurdie, H. F., *Phase Diagrams for Ceramists*, Vol. I. American Ceramic Society Inc., Columbus, OH, 1964, p. 156.
3. Ervin, G. Jr, Oxidation behaviour of silicon carbide. *J. Am. Ceram. Soc.*, **41** (1958) 351.
4. Hayashi, T., Nishio, H. & Ayuzawa, N., The behaviour of alkali to alumina. *Interceram, Special Issue*, **32** (1983) 68–71.
5. Turkdogan, E. T., *Physical Chemistry of High Temperature Technology*. Academic Press, New York, 1980.
6. Carr, A. J. & Hendry, A., Comments on Kaufman's Model for Gibbs Energy of Formation for Beta-sialon. Report to SERC, GR/D/98044, Swindon, UK, 1989.

Appendix: Thermodynamic Data

Plot	Equation	$RT \ln P_{O_2}$ (kJ)	Ref.
1	$2C + O_2 = 2CO(g)$	$-228{\cdot}79 - 0{\cdot}1715T + 0{\cdot}0383T \log P_{CO}$	5
2	$4K(g) + 8SiO_2 + O_2 = 2KS_4(l)$	$-1603{\cdot}35 + 0{\cdot}5682T - 0{\cdot}0766T \log P_K$	1
3	$4K(g) + 3{\cdot}33KAS_6(l) + 0{\cdot}67A_3S_2 + O_2 = 5{\cdot}33KAS_4(s)$	$-2212{\cdot}97 + 0{\cdot}8732T - 0{\cdot}0766T \log P_K$	1
4	$4K(g) + 2Al_2O_3 + 2KAS_4(s) + O_2 = 4KAS_2(s)$	$-1724{\cdot}69 + 0{\cdot}5774T - 0{\cdot}0766T \log P_K$	1
5	$4K(g) + 4A_3S_2 + O_2 = 2KAS_4(s) + 10Al_2O_3$	$-1843{\cdot}10 + 0{\cdot}5531T - 0{\cdot}0766T \log P_K$	1
6	$0{\cdot}45K(g) + 0{\cdot}0118Si_{76}N_{100}O_2 + O_2 = 0{\cdot}22KS_4(l) + 0{\cdot}59N_2$	$-656{\cdot}90 + 0{\cdot}0565T - 0{\cdot}0086T \log P_K + 0{\cdot}0113T \log P_{N_2}$	1
6A	$0{\cdot}57K(g) + 0{\cdot}57Si_2N_2O + O_2 = 0{\cdot}29KS_4(l) + 0{\cdot}57N_2$	$-759{\cdot}00 + 0{\cdot}1490T - 0{\cdot}0109T \log P_K + 0{\cdot}0109T \log P_{N_2}$	1
7	$0{\cdot}40K(g) + 0{\cdot}20Si_4Al_2O_2N_6 + O_2 = 0{\cdot}20KAS_4(s) + 0{\cdot}60N_2$	$-770{\cdot}17 + 0{\cdot}1109T - 0{\cdot}0077T \log P_K + 0{\cdot}0115T \log P_{N_2}$	1, 5, 6
8	$0{\cdot}67K(g) + 0{\cdot}22Si_3Al_3O_3N_5 + O_2 = 0{\cdot}33KAS_2(s) + 0{\cdot}56N_2$	$-841{\cdot}44 + 0{\cdot}1500T - 0{\cdot}0128T \log P_K + 0{\cdot}0106T \log P_{N_2}$	1, 5, 6
9	$0{\cdot}67Si_2N_2O + O_2 = 1{\cdot}33SiO_2(s) + 0{\cdot}67N_2$	$-617{\cdot}99 + 0{\cdot}0728T + 0{\cdot}0128T \log P_{N_2}$	1
10	$0{\cdot}26K(g) + 0{\cdot}21Si_4Al_2O_2N_6 + O_2 = 0{\cdot}13KAS_6(l) + 0{\cdot}03A_3S_2 + 0{\cdot}62N_2$	$-713{\cdot}96 + 0{\cdot}0812T - 0{\cdot}0050T \log P_K + 0{\cdot}0119T \log P_{N_2}$	1, 5, 6
11	$0{\cdot}30K(g) + 0{\cdot}25Si_3Al_3O_3N_5 + O_2 = 0{\cdot}15KAS_4(s) + 0{\cdot}07A_3S_2 + 0{\cdot}62N_2$	$-741{\cdot}11 + 0{\cdot}1029T - 0{\cdot}0057T \log P_K + 0{\cdot}0118T \log P_{N_2}$	1, 5, 6
12	$0{\cdot}36K(g) + 0{\cdot}24Si_3Al_3O_3N_5 + O_2 = 0{\cdot}18KAS_4(s) + 0{\cdot}18Al_2O_3 + 0{\cdot}61N_2$	$-761{\cdot}15 + 0{\cdot}1111T - 0{\cdot}0070T \log P_K + 0{\cdot}0116T \log P_{N_2}$	1, 5, 6
13	$0{\cdot}06Si_{76}N_{100}O_2 + O_2 = 2{\cdot}11Si_2N_2O + 0{\cdot}67N_2$	$-281{\cdot}17 - 0{\cdot}2661T + 0{\cdot}0128T \log P_{N_2}$	1
14	$25{\cdot}33Si_3N_4 + O_2 = Si_{76}N_{100}O_2 + 0{\cdot}67N_2$	$-7684{\cdot}10 + 4{\cdot}4352T + 0{\cdot}0128T \log P_{N_2}$	1
15	$1{\cdot}33Si_3N_4 + O_2 = 2Si_2N_2O + 0{\cdot}67N_2$	$-670{\cdot}71 - 0{\cdot}0180T + 0{\cdot}0128T \log P_{N_2}$	1
16	$3Si(l) + 2N_2 = Si_3N_4$	$T_{Dissociation} = 924{\cdot}60/(0{\cdot}4494 - 0{\cdot}0383 \log P_{N_2})$	1
17	$4Si(l) + 2N_2 + O_2 = 2Si_2N_2O$	$-1903{\cdot}35 + 0{\cdot}5812T - 0{\cdot}0383T \log P_{N_2}$	1
$z = 2$	$4Si(l) + 2Al(l) + 3N_2 + O_2 = Si_4Al_2O_2N_6$	$-2598{\cdot}08 + 0{\cdot}8681T + 0{\cdot}0574T \log P_{N_2}$	6
$z = 3$	$2Si(l) + 2Al(l) + 1{\cdot}67N_2 + O_2 = 0{\cdot}67Si_3Al_3O_3N_5$	$-1978{\cdot}48 + 0{\cdot}5751T + 0{\cdot}0319T \log P_{N_2}$	6